Solar Phys (2019) 294:170
https://doi.org/10.1007/s11207-019-1558-8

Assessing the Performance of EUHFORIA Modeling the Background Solar Wind

Jürgen Hinterreiter [1,2] · Jasmina Magdalenic[3] · Manuela Temmer[2] · Christine Verbeke[4] · Immanuel Christopher Jebaraj[3,4] · Evangelia Samara[3,4] · Eleanna Asvestari[2,5] · Stefaan Poedts[4] · Jens Pomoell[5] · Emilia Kilpua[5] · Luciano Rodriguez[3] · Camilla Scolini [3,4] · Alexey Isavnin[4]

Received: 19 August 2019 / Accepted: 15 November 2019 / Published online: 5 December 2019

Abstract In order to address the growing need for more accurate space-weather predictions, a new model named EUHFORIA (EUropean Heliospheric FORecasting Information Asset) was recently developed. We present the first results of the performance assessment for the solar-wind modeling with EUHFORIA and identify possible limitations of its present setup. Using the basic EUHFORIA 1.0.4 model setup with the default input parameters, we modeled background solar wind (no coronal mass ejections) and compared the obtained results with *Advanced Composition Explorer* (ACE) *in-situ* measurements. For the purposes of sta-

✉ J. Hinterreiter
juergen.hinterreiter@oeaw.ac.at

J. Magdalenic
jasmina.magdalenic@oma.be

M. Temmer
manuela.temmer@uni-graz.at

C. Verbeke
Christine.Verbeke@kuleuven.be

I.C. Jebaraj
immanuel.jebaraj@oma.be

E. Samara
evangelia.samara@oma.be

E. Asvestari
eleanna.asvestari@helsinki.fi

S. Poedts
stefaan.poedts@kuleuven.be

J. Pomoell
jens.pomoell@helsinki.fi

E. Kilpua
emilia.kilpua@helsinki.fi

L. Rodriguez
luciano.rodriguez@observatory.be

C. Scolini
camilla.scolini@kuleuven.be

tistical study we developed a technique of combining daily EUHFORIA runs into continuous time series. The combined time series were derived for the years 2008 (low solar activity) and 2012 (high solar activity), from which *in-situ* speed and density profiles were extracted. We find for the low-activity phase a better match between model results and observations compared to the high-activity time interval considered. The quality of the modeled solar-wind parameters is found to be rather variable. Therefore, to better understand the results obtained we also qualitatively inspected characteristics of coronal holes, *i.e.* the sources of the studied fast streams. We discuss how different characteristics of the coronal holes and input parameters to EUHFORIA influence the modeled fast solar wind, and suggest possibilities for the improvement of the model.

Keywords Coronal Holes · Magnetic fields, Models · Solar Wind · Magnetohydrodynamics

1. Introduction

The solar wind is a continuous flow of charged particles propagating outward from the hot corona of the Sun into interplanetary space. The speed measured at 1 AU heliocentric distance covers generally a range between 300 and 800 $\mathrm{km\,s^{-1}}$, consisting of slow solar wind and of high-speed solar-wind streams that have different characteristics and sources (*e.g.* Schwenn, 2006; Cranmer, Gibson, and Riley, 2017).

The sources of the slow solar wind are closed magnetic-field regions of coronal loops, active regions, coronal hole (CH) boundaries, and also streamers and pseudostreamers (Cranmer, Gibson, and Riley, 2017). On the other hand, fast solar wind emanates from open magnetic-field regions, CHs, along which ionized atoms (mainly protons and alpha-particles) and electrons may easily escape to interplanetary space. CHs are localized regions of low density and low temperature in the solar corona that are generally slowly evolving and may persist for several solar rotations (Schwenn, 2006). However, where exactly within the CH the high-speed component of the solar wind gets accelerated is not well understood and is the subject of numerous studies.

High-speed streams from CHs interact with the slower solar wind ahead causing compression regions that can lead to geomagnetic storms, and the fast stream following the compression region with Alfvénic fluctuations can prolong substantially the recovery phase of the storm (*e.g.* Tsurutani and Gonzalez, 1987). It is well acknowledged that during the maximum phase of the solar-cycle space weather is affected mostly by transient coronal mass ejections (CME: *e.g.* Webb and Howard, 2012), however, during the declining and minimum-activity phases high-speed streams have significant impact (Tsurutani *et al.*, 2006;

A. Isavnin
alexey.isavnin@kuleuven.be

1 Space Research Institute, Austrian Academy of Sciences, Graz, Schmiedlstraße 6, 8042 Graz, Austria

2 Institute of Physics, University of Graz, Universitätsplatz 5, 8010 Graz, Austria

3 Solar–Terrestrial Centre of Excellence–SIDC, Royal Observatory of Belgium, 1180 Brussels, Belgium

4 Centre for Mathematical Plasma Astrophysics (CmPA), KU Leuven, 3001 Leuven, Belgium

5 Department of Physics, University of Helsinki, P.O. Box 64, 00014 Helsinki, Finland

Richardson and Cane, 2012; Kilpua *et al.*, 2017). At all phases of the solar cycle, high-speed solar-wind streams have also a paramount impact causing enhancements of Van Allen belt electron fluxes to relativistic electrons (*e.g.* Paulikas and Blake, 1979; Jaynes *et al.*, 2015; Kilpua *et al.*, 2015), and they strongly structure interplanetary space, which is an important factor when studying and forecasting the propagation of CMEs. In general the morphology, area, and location of CHs play a major role in the properties of the resulting compression region, duration and speed of the fast stream, and thus, its space-weather impact level (*e.g.* Vršnak, Temmer, and Veronig, 2007; Garton, Murray, and Gallagher, 2018). For example, statistical studies have shown that the equatorial parts of CHs are the main contributors to the fast solar-wind streams measured at Earth (see, *e.g.*, Karachik and Pevtsov, 2011; Hofmeister *et al.*, 2018) and that the speed of the solar wind at Earth increases with increasing CH area (*e.g.* Rotter *et al.*, 2012; Nakagawa, Nozawa, and Shinbori, 2019). We note that with the evolution of a CH over time, also the associated *in-situ* measured solar-wind parameters, can change (*e.g.* Heinemann *et al.*, 2018).

During the last decades a vast number of solar-wind models were developed, employing different approaches, and the majority of them aimed to predict the background solar wind at the Earth. Some of the models have physics-based algorithms such as ENLIL (Odstrčil and Pizzo, 1999) or MHD about a Sphere (MAS: Linker *et al.*, 1999) using synoptic photospheric magnetic-field maps as input. Also empirical relations between observed areas of CHs and measured solar-wind speeds at 1 AU are applied (Vršnak, Temmer, and Veronig, 2007; Rotter *et al.*, 2012; Reiss *et al.*, 2016; Bussy-Virat and Ridley, 2014; Riley *et al.*, 2017; Owens, Riley, and Horbury, 2017). Simple persistence models employ *in-situ* measurements shifted forward by variable times depending on the spacecraft location (*e.g.* Opitz *et al.*, 2009; Owens *et al.*, 2013). Some models use the MHD codes for the coronal and the heliospheric domain (*e.g.* Den *et al.*, 2015; van der Holst *et al.*, 2014; Feng *et al.*, 2012), while others make use of the WSA model (Arge and Pizzo, 2000) for the coronal domain and MHD codes for the heliospheric domain (*e.g.* Odstrčil and Pizzo, 1999; Wiengarten *et al.*, 2013; Shiota *et al.*, 2014; Merkin *et al.*, 2016). A good overview on the existing models can be found in MacNeice *et al.* (2018). The performances of the different solar-wind models, in comparison to actual measurements, reveal on average root-mean-square-errors of around $100-150\ \mathrm{km\,s^{-1}}$ in the wind speed and time shifts in the arrival of the peak speed of about one day and up to three days (see, *e.g.*, Owens *et al.*, 2008; MacNeice, 2009; Gressl *et al.*, 2014; Jian *et al.*, 2015; Reiss *et al.*, 2016; Temmer, Hinterreiter, and Reiss, 2018). In general, model performances decrease with increased solar-activity phases as CMEs frequently disturb the interplanetary space. Especially empirical solar-wind models are not able to cope with those disturbances, but also for numerical models preconditioning is an important aspect that needs to be taken into account (Temmer *et al.*, 2017).

In order to address the growing need for more accurate space-weather predictions, a new model named EUHFORIA (EUropean Heliospheric FORecasting Information Asset) was recently developed (Pomoell and Poedts, 2018). In the following we present the first performance assessment of the solar-wind model and identify possible caveats related to complex solar-surface situations. As this work's focus is on the benchmark study and first evaluation of the new model, we compare modeled solar wind by EUHFORIA only with *in-situ* observations. This comparison with observations is a necessary first step for a model validation, and testing of EUHFORIA's performance in solar-wind modeling against other solar-wind models will be presented in the follow-up publication.

In Section 2 we introduce EUHFORIA with its default parameters and explain how we obtain a full time series from individual model runs. Section 3 deals with the comparison of the model results with *in-situ* measurements and addresses some limitations of the basic setup of EUHFORIA. In Section 4 we summarize our results.

2. Solar-wind modeling with EUHFORIA

EUHFORIA is a physics-based simulation tool consisting of three essential parts: a coronal model, a heliospheric model, and an eruption model. The main purpose of the coronal model is to provide realistic plasma conditions of the solar wind at the interface radius $r = 0.1$ AU between the coronal and heliospheric model. The heliospheric model computes the time-dependent evolution of the plasma from the interface radius by numerically solving the MHD equations with the boundary conditions provided by the coronal model. For simulating transient events, CMEs are injected at the interface radius of the eruption model. Presently EUHFORIA shares similarities with the well-established solar-wind/ICME model for the inner heliosphere WSA-ENLIL (Odstrcil, Riley, and Zhao, 2004). An important feature of EUHFORIA is its flexibility. The three models, heliospheric, coronal, and eruption, are fully autonomous and each part of EUHFORIA can be easily replaced by other models (more details are given by Pomoell and Poedts, 2018; Scolini *et al.*, 2018).

EUHFORIA presently provides daily runs using hourly updated standard synoptic *Global Oscillation Network Group* (GONG) magnetograms and adapt GONG maps. In this way the central part of the magnetogram, used by EUHFORIA, is updated daily. For the purpose of the statistical studies and easier comparison with *in-situ* observations, we combine daily runs in order to obtain single time series (for a detailed description see Section 2.2).

In the present study we used the EUHFORIA 1.0.4 version of the model, and we focus on the coronal and heliospheric model, in order to assess how well EUHFORIA simulates the background solar wind. For this study, we considered two phases of solar activity: one year during minimum in 2008 and another year during maximum in 2012.

2.1. The Input Parameters and Setup of EUHFORIA

As this is the first study of solar-wind modeling with EUHFORIA, we employed the so-called default setup, which uses default values for the input parameters. For the coronal part of the model, we use synoptic magnetograms from GONG, and the potential-field source-surface (PFSS) model (Altschuler and Newkirk, 1969) to simulate the magnetic field up to heights of 2.6 $R_\odot$ (so-called source-surface height). This is combined with the Schatten current sheet (SCS) model (Schatten, Wilcox, and Ness, 1969) starting from the height of 2.3 $R_\odot$ and that extends up to 0.1 AU. By overlapping the two models, a smoother transition between the lower coronal PFSS and upper coronal SCS model is obtained (see Pomoell and Poedts, 2018; McGregor *et al.*, 2008). To determine the solar-wind plasma parameters at the inner boundary of the heliospheric model we use the empirical Wang–Sheeley–Arge model (Arge *et al.*, 2003), which is described below.

In EUHFORIA the solar-wind speed depends on several parameters and the functional form of the empirical relation can be selected by the user. In this study we have employed the expression in the form

$$v(f,d) = v_0 + \frac{v_1}{(1+f)^\alpha}\left[1 - 0.8\exp(-(d/w)^\beta)\right]^3, \tag{1}$$

where f and d are the flux-tube expansion factor and the angular distance from the footpoint of each open field line to the nearest CH boundary, respectively. The parameters in Equation 1 are set to $v_0 = 240$ km s^{-1}, $v_1 = 675$ km s^{-1}, $\alpha = 0.222$, $\beta = 1.25$ and $w = 0.02$ rad. For a more detailed description see Equation 2 of Pomoell and Poedts (2018). Since the original WSA relation is designed to provide the wind speed at Earth, and as the solar wind continues to accelerate beyond the inner boundary in the heliospheric MHD model, we have

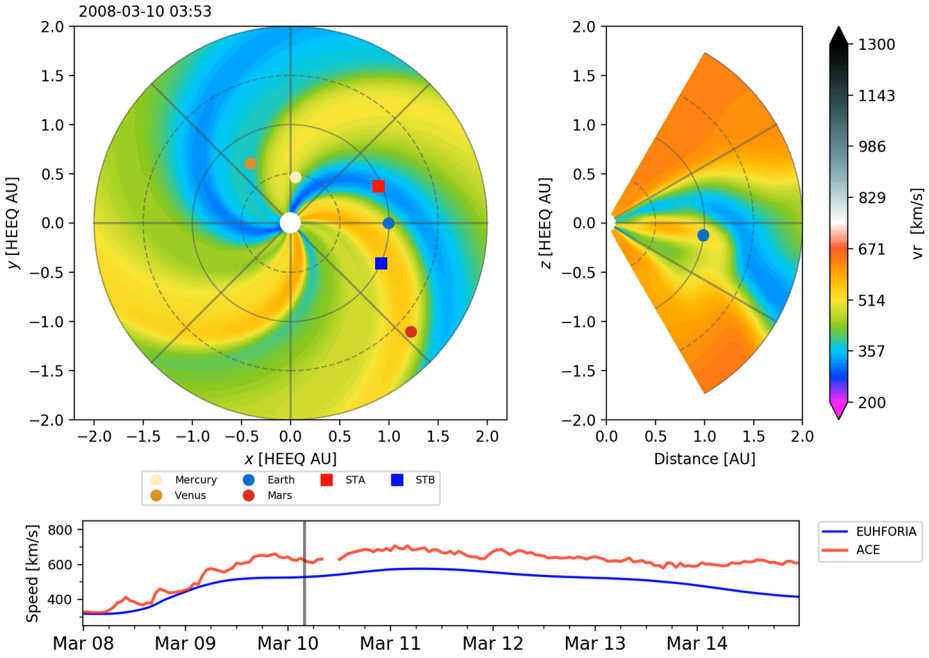

Figure 1 Snapshot of the background solar-wind radial speed modeled by EUHFORIA. The *top-left panel* shows the MHD solution in the heliographic equatorial plane, and the *right panel* shows the meridional plane cut that includes the Earth (*blue circle*). The *lower panel* shows comparison of the modeled and observed solar wind by EUHFORIA and ACE, respectively.

additionally subtracted 50 km s^{-1} to avoid a systematic overestimate of the wind speed. To compensate for solar rotation, which is not included in the magnetic-field model, we rotate the solar-wind speed map at the inner boundary by 10°. We have also limited the minimum and the maximum solar-wind speed at the inner boundary to 275 and 625 km s^{-1}, respectively (according to McGregor *et al.*, 2011). In addition to the wind speed, the remaining MHD variables need to be determined. While the topology of the magnetic field is directly obtained from the SCS model, the magnitude of the solar-wind magnetic field is set to be directly proportional to the speed. The plasma number density is given by

$$n = n_{\mathrm{fsw}}(v_{\mathrm{fsw}}/v_r)^2, \tag{2}$$

with the number density of the fast solar wind $n_{\mathrm{fsw}} = 300$ cm^{-3} (*e.g.* Bougeret, King, and Schwenn, 1984; Venzmer and Bothmer, 2018), the fast solar-wind speed $v_{\mathrm{fsw}} = 675$ km s^{-1}, and v_r coming from the empirical speed prescription. The maximum value $v_{\mathrm{fsw}} = 675$ km s^{-1} is considered to be in the solar-wind plasma with a magnetic field of 300 nT. For more details see Equation 4 of Pomoell and Poedts (2018).

Finally, we use a constant plasma thermal pressure of 3.3 nPa, at the inner boundary, which is in accordance with the fast solar-wind temperature of about 0.8 MK. The angular resolution of the daily runs in this study was 4°, while 512 grid cells were chosen in the radial direction to cover the 0.1 to 2 AU domain.

An example of the background solar-wind speed modeled by EUHFORIA, for the time interval of seven days in March 2008, is presented in Figure 1. The two top panels (the heliographic equatorial and the meridional plane cuts plotted in the left and right panels,

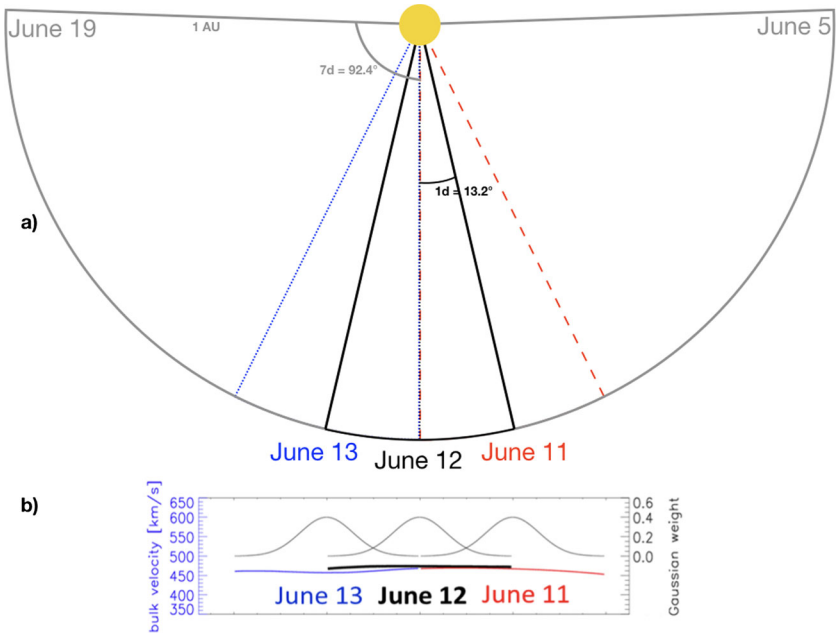

Figure 2 Schematic representation of combining EUHFORIA model output for consecutive days. (**a**) *Different colors* represent the selected range ($\pm 13.2°$ from the solar central region) for each day. Indicated in *gray* is the full range ($\pm 92.4°$) provided by the model. (**b**) Gaussian weight used for the model properties shown for three individual days.

respectively) show that the Earth has entered a region of extended fast flow. The time of the snapshot is also marked by the black vertical line in the bottom panel, which shows a comparison between the *in-situ* observations and modeled solar-wind speed. For this time period, we note a good match between the modeled solar wind by EUHFORIA and the *in-situ* measurements (see bottom panel of Figure 1).

2.2. Combining Individual Runs and Obtaining EUHFORIA Time Series

For the systematic testing of the background solar wind at the Earth we used EUHFORIA daily runs, *i.e.* model outputs with default parameters. We focus on the evaluation of the EUHFORIA's prediction at the Earth (although any other point could be also considered for the comparison) because of the availability of the data and the general interest in evaluating the performance of the model at the Earth due to socio–economic reasons. The EUHFORIA daily runs are based on standard synoptic GONG magnetograms (the selected time was about 23:30 UT each day) and do not include modeling of possible CMEs. The study comprises two complete years: 2008 and 2012. We consider that each daily run, based on one magnetogram input, simulates the background solar wind at the heliocentric distance of 1 AU over a total time span of 14 days (± 7 days) covering $\pm 92.4°$ in longitude (see gray slice in Figure 2) with a temporal resolution of ten minutes. The central region of the Sun has the magnetic-field information with the lowest projection effects, and it is thus the most reliable part of the magnetogram. To combine the individual daily runs, which overlap in time, we therefore developed a method containing information with highest weight on the central region of the Sun. The central region is defined as ± 1 day around the central meridian (0°)

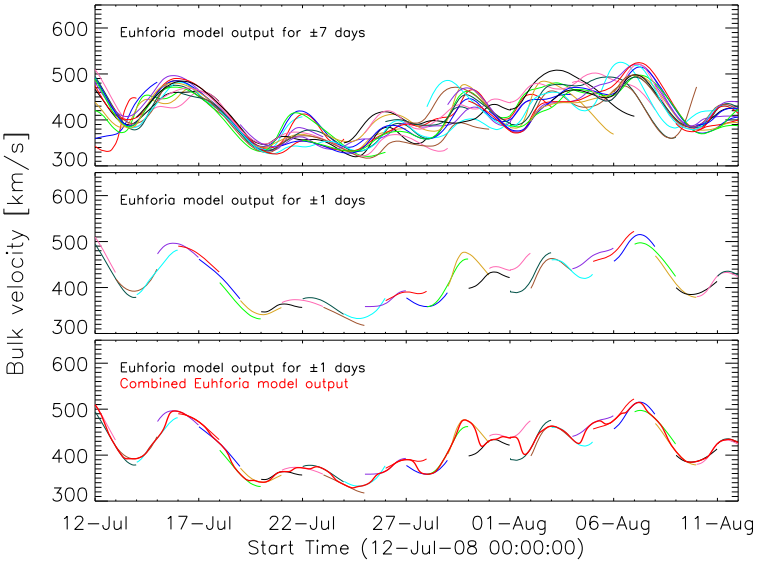

Figure 3 Solar-wind speed from July to August 2008. *Top panel*: Full EUHFORIA model output (± seven days). *Middle panel*: EUHFORIA model output limited to ± one day. *Bottom panel*: Model output (different colors for each daily run) and resulting time series (*thick red*).

as given in the schematic drawing in Figure 2a. The weighting of each curve is done by a Gaussian distribution with the central part receiving the strongest weight (see Figure 2b). We note that the described procedure does not include blending of the entire 3D solutions, but only combining the solutions in order to extract a time series at on exact location in space at the Earth. Studies that include CME modeling with EUHFORIA do not combine the runs (see Scolini *et al.*, 2019).

In Figure 3 we demonstrate how the method was applied. The top panel of Figure 3 shows the solar-wind speed modeled by EUHFORIA for the full model output (± seven days). Different colors represent results from 32 daily runs. As can be seen, the simulated solar-wind speeds for consecutive days may show significant offsets. In order to obtain a smooth time series we first limit the curves in time to ± one day (middle panel) and then combine them by using a Gaussian distribution (*cf.* Figure 2b). The obtained combined time series which is used for the analysis is given in the bottom panel of Figure 3 by the thick red curve. We also tested different limits of temporal ranges for the individual runs; *e.g.* ± three days, in order to check the quality of the method when combining individual runs. The resulting combined time series are rather similar and slightly more smoothed compared to using a time range limit of ± one day.

We evaluate how the combined time series for the modeled solar-wind speed are affected when shifting the weighting to a region different from the central part of the Sun. With this, we take into account that compared to the central region of the magnetogram the eastern or western region could influence more strongly the simulated solar wind. Figure 4 shows the results for the shifted weighting. One can observe clear differences between the combined time series; however, when inspecting longer time ranges the general trend is retained.

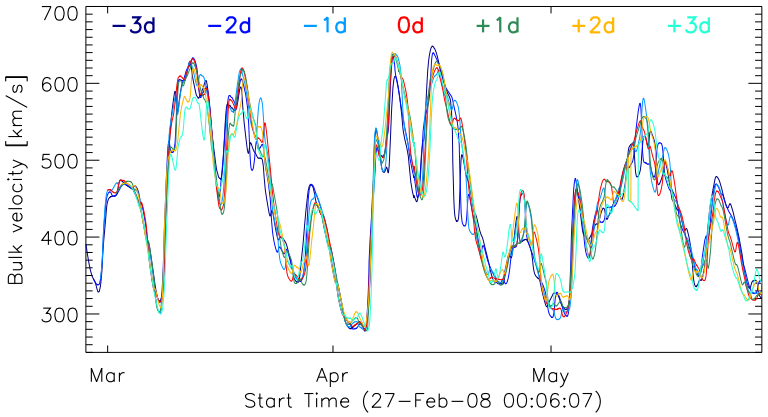

Figure 4 Comparison of different shifts of the central region. The *red curve* (*0d*) represents the central region used for the individual runs. *−3d* indicates that the central region is shifted three days to the East while *+3d* indicates a shifting of the central region to the West.

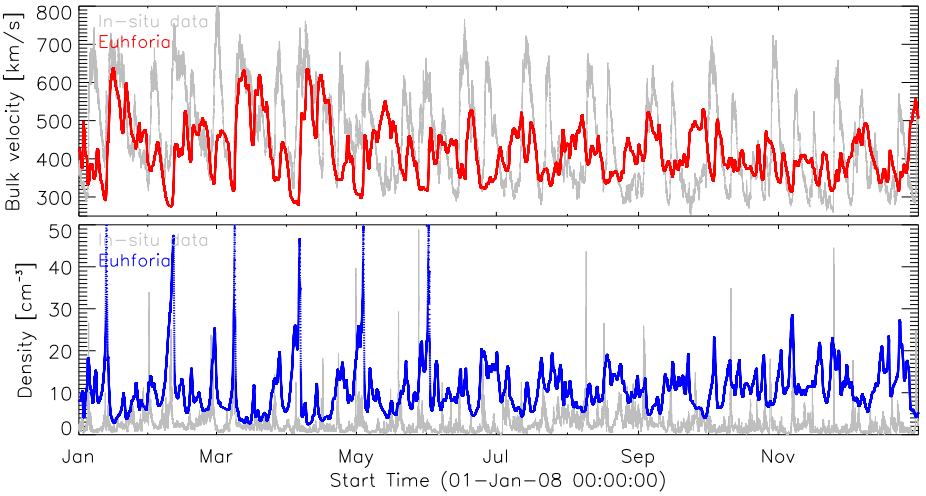

Figure 5 EUHFORIA model output (*red*: velocity, *blue*: density) in comparison to *in-situ* measurements (*gray*) for 2008. *Top panel*: Solar-wind bulk velocity. *Bottom panel*: Solar-wind density.

3. Comparison of *in-situ* Observations and Modeled Solar Wind

In order to assess the performance of the model we chose two intervals of different solar-activity levels. At first, a quiet period during 2008 is considered, for which only three interplanetary coronal mass ejections (ICMEs), at the end of the year, were reported in the near-Earth solar wind according to the Richardson and Cane ICME list (Richardson and Cane, 2010, see www.srl.caltech.edu/ACE/ASC/DATA/level3/icmetable2.htm). This period can serve as a benchmark time interval for the model performance as it almost optimally represents the background solar wind without significant transient perturbations. A second interval considered covers the year 2012, a period with a rather high level of solar activity during which 35 ICMEs are reported (*cf.* Richardson and Cane ICME list). In order to evaluate how well

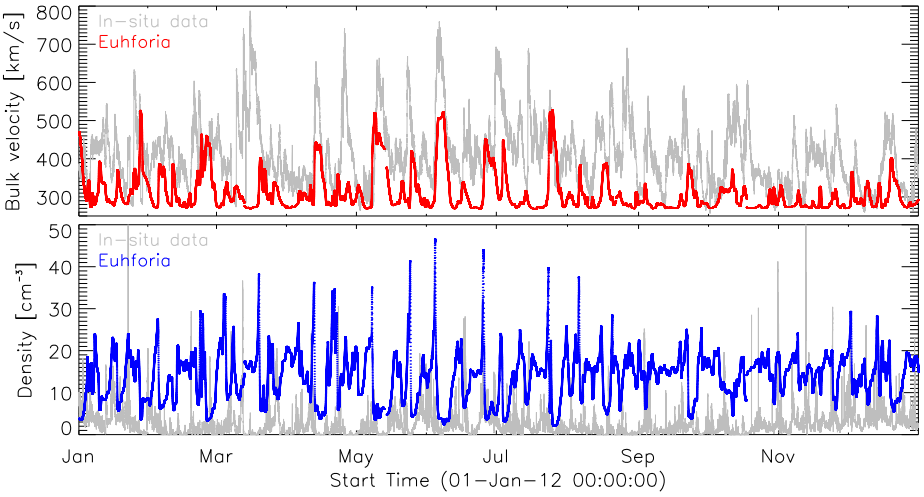

Figure 6 EUHFORIA model output (*red*: velocity, *blue*: density) in comparison to *in-situ* measurements (*gray*) for 2012. *Top panel*: Solar-wind bulk velocity. *Bottom panel*: Solar-wind density.

EUHFORIA models the background solar wind, we compare the combined time series (see Section 2.2) with the *in-situ* measured plasma speed and density as provided by the *Solar Wind Electron, Proton and Alpha Monitor* onboard the *Advanced Composition Explorer* (ACE/SWEPAM: McComas *et al.*, 1998).

Figures 5 and 6 show the results obtained for the years 2008 and 2012. The gray curves represent observed values by ACE, while red and blue curves represent modeled values of the solar-wind speed and density, respectively. The statistics presented of the background solar wind modeled with EUHFORIA show on average lower values of the modeled solar-wind speed than the *in-situ* measured velocity. On the other hand the modeled solar-wind density is considerably higher than the observed one. In the present setup of EUHFORIA these two solar-wind plasma parameters are coupled (see Equation 2), and improved modeling of the solar-wind speed will also result in a better modeled solar-wind density. We also noticed that the correlation between modeled and observed values is significantly better in the first half of the year 2008 (Figure 5). In the second half of the year 2008, the maximum speeds for the fast solar-wind speed are not well modeled by EUHFORIA, and also the minimum values are significantly different, *i.e.* larger than the observed ones. For the year 2012 the discrepancies between the modeled values and observations are more pronounced. Nevertheless, periods of lower wind speeds during 2012 are rather well reproduced, which might be simply a consequence of a very low wind speed in general obtained for this year.

The *in-situ* solar-wind speed, for both years studied, was also compared to the individual daily runs in order to assess the probability of artificially enhanced or reduced fast-wind flows due to combining of the daily runs (Section 2.2). In the two studied years we found only one case of the fast solar wind that was observed in the majority of the daily runs but not in the combined time series (around 22 August 2012). The opposite cases, where the combined time series show significant increase of the solar-wind speed that was not modeled in the majority of the relevant daily runs, were not found.

As a consequence of the, on average, underestimated solar-wind speed modeled by EUHFORIA, fast flows arrive with a systematic delay in time. The amount of delay depends on the difference between the modeled and observed wind speed. For example, the fast so-

lar wind with average speed of 600 km s^{-1} will need about 2.9 days to arrive at the Earth, while those of about 500 km s^{-1} will need about 3.5 days. In this case the induced latency of the modeled solar wind will be about 14 hours. We observe the influence of this effect particularly strongly in the second half of the year 2008 (Figure 5).

3.1. Evaluation of Modeling Results

In order to evaluate the EUHFORIA model performance we present hit–miss statistics using two different methods for comparing measured and modeled results. We also compare the minimum and maximum phase of the results and give initial results on the effects of different input parameters for the model. In this analysis we focus only on the solar-wind velocity.

3.1.1. Hit–Miss Statistics by Automatic Peak–Peak Matching Method

To evaluate the model performance, we calculate continuous variables (*e.g.* root-mean-squared error: RMSE) and apply an event-based approach for detecting the maxima (peak-finding algorithm) in the solar-wind observations. For the event-based approach we used an automatic peak-finding algorithm. To be defined as a peak, certain properties (minimum speed = 350 km s^{-1}, minimum gradient = 60 km s^{-1}, for further details see Reiss *et al.*, 2016) have to be fulfilled. A hit is found if the modeled peak appears within a time window of $\pm$ two days around the measured peak, and a miss if the modeled peak is out of this time window. If the peak is found in the combined time series of EUHFORIA and not in observations, we consider this a false alarm.

Since the study also encompasses the year 2012 with a high level of solar activity, it was necessary to isolate intervals with possible ICMEs in the *in-situ* observations. The vertical pink lines in Figure 7 indicate the times of CME occurrences according to the CME list (Richardson and Cane, 2010). We note that for 2008 only three ICMEs were reported, while for 2012 there are 35 reported events.

For both years under study we obtain a similar result regarding the RMSE, which is about 125 km s^{-1}. As can be seen from Figure 7, in 2008 (top panel), 39 solar-wind peaks are detected in the EUHFORIA combined time series and 43 in the *in-situ* data. Applying the automatic peak-finding algorithm method, we obtain 18 hits, 21 false alarms, and 25 misses. In 2012 (bottom panel in Figure 7), the EUHFORIA combined time series shows 21 peaks and 38 are detected in the *in-situ* observations. This corresponds to 14 hits, 7 false alarms, and 24 misses. As this is a rather poor result we inspect the solar-wind profiles (observed and modeled) in more detail and investigate the reason for the poor performance.

3.1.2. Hit–Miss Statistics by Manual Peak–Peak Matching Method

The *in-situ* observations frequently show several subsequent local maxima of the solar-wind speed associated with a single fast flow generally originating from a large and extended, in latitude or in longitude or both, CH. In such a case the automatic peak-finding algorithm finds several peaks, and it is not possible to make a one-to-one identification with the usually smooth increase of the solar-wind speed modeled by EUHFORIA. In order to better understand such long-lasting flows and to unambiguously relate modeled and observed velocity peaks with each other, we checked the development of the CHs on the Sun two days before and three days after the CH started crossing the central meridian (see Figure 8). For this purpose we analyzed automatic CH areas detected by the CHIMERA software (Garton, Gallagher, and Murray, 2018) and CH drawings (see Figure 8).

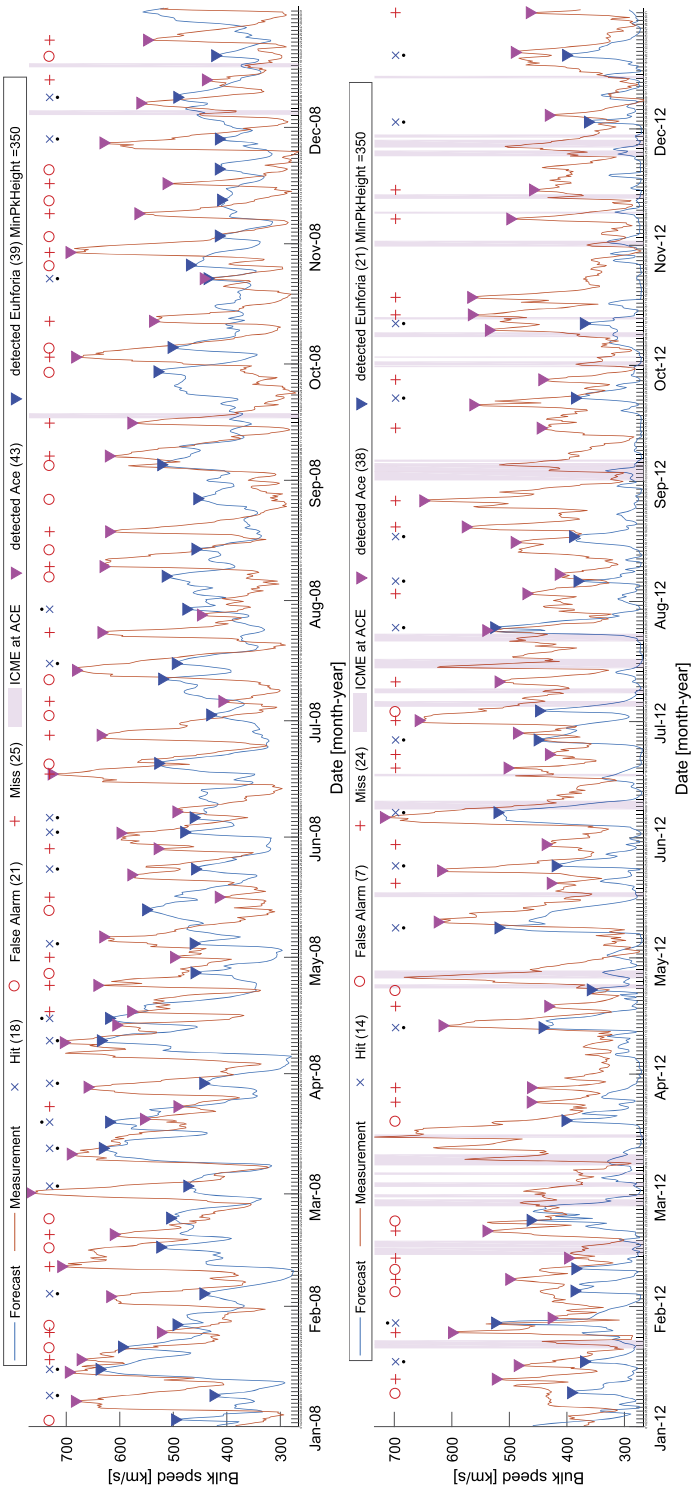

Figure 7 EUHFORIA modeled solar-wind bulk velocity (*blue*) in comparison to *in-situ* measurements (*orange*) for 2008 (*top*) and 2012 (*bottom*) using a peak-finding algorithm. The *pink vertical bars* indicate times of CME occurrences according to Richardson and Cane (2010).

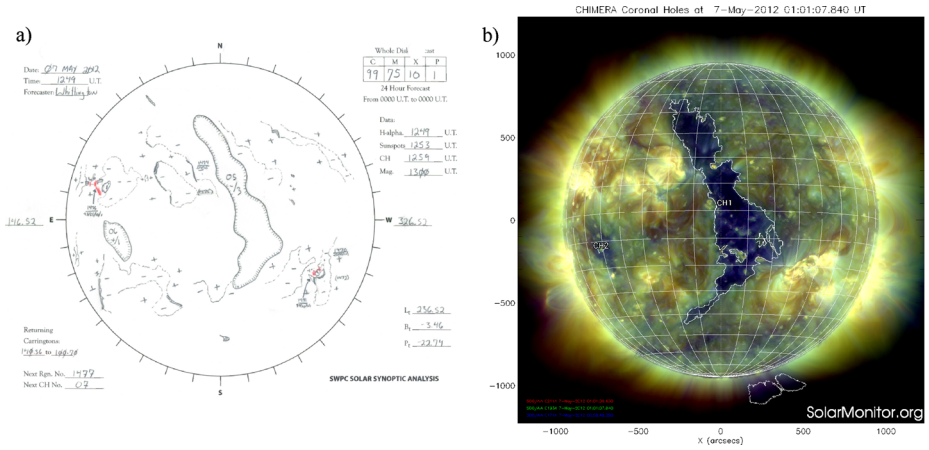

Figure 8 (**a**) Drawing of the solar-surface features for 7 May 2012 provided by NOAA. The CH is identified using EUV imagery from spacecraft while the polarity of the CH is obtained from magnetograms. (**b**) Detection of the CH on the same day, by the CHIMERA tool (based on three wavelengths 211, 193, 171 Å). The image was obtained from Solar Monitor.

As for the automatic method, the intervals corresponding to ICME arrivals, reported in a list by Richardson and Cane (2010) and observed *in-situ*, were excluded from the evaluation. In addition, peaks in the *in-situ* measured solar-wind speed that could not be related to CHs were also excluded from the statistical study. We considered observed and modeled solar-wind peaks to be associated, *i.e.* a hit, if the increase started more or less simultaneously and the peak was achieved within two days after the peak as modeled by EUHFORIA. When the modeled solar-wind increase did not have a counterpart in the *in-situ* observations we considered this a false alarm, and when the observed fast flow was not reproduced by EUHFORIA we consider to have a miss.

The manual identification of the CHs and associated fast flows shows 17 hits, 12 misses, and 6 false alarms for 2008 and 13 hits, 18 misses, and no false alarms for 2012. We note that these results reveal a significantly smaller number of false alarms and misses in comparison to the automatic method. This indicates that the CH development and its shape have strong influence on the fast solar-wind speed profile measured at 1 AU.

3.1.3. Solar-Cycle Dependence

In Figures 5 and 6 it can be seen that the solar wind modeled by EUHFORIA matches much better for the interval of the minimum solar activity in 2008. This may have several reasons. During low levels of solar activity the magnetic field, the main input for the PFSS extrapolation in EUHFORIA, changes less dynamically than during high levels of solar activity, which can result in a more reliable modeling of the solar-wind flow. Also, the interplanetary measurements are not disturbed by transient events, which are much less frequent compared to solar-maximum activity, and the solar-wind flow is more persistent (Owens *et al.*, 2013; Temmer, Hinterreiter, and Reiss, 2018).

Figure 5a shows for 2008, on average, rather good model results of the minimum and maximum solar-wind speed, and the majority of fast flows associated with equatorial CHs are well reproduced. However, we also found an exception where the *in-situ* observations show a recurrent fast flow (ten rotations) associated with a well-defined equatorial CH that

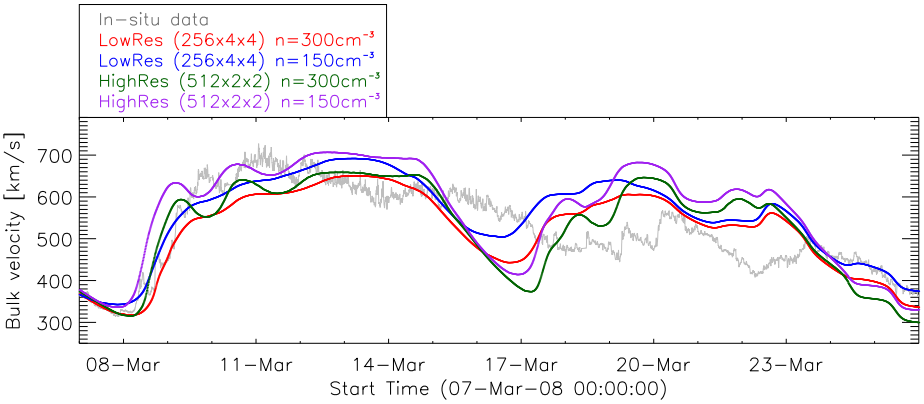

Figure 9 Comparison of model runs with different settings. High/default density: 300 cm^{-3}, low/default resolution: 4° in longitude and latitude with 256 radial cells (256 × 30 × 90). Low density: 150 cm^{-3}, high resolution: 2° in longitude and latitude with 512 radial cells (512 × 60 × 180).

was modeled by EUHFORIA only at the beginning of the year 2008. We believe that modeling of the solar wind originating from this particular CH is highly influenced by the CH characteristics and development in location, size, and shape.

During a high level of solar activity the magnetic field is very complex, and it is known that the amount of low-latitude open flux may be significantly underestimated by the PFSS model (*e.g.* MacNeice, Elliott, and Acebal, 2011). Underestimating the open flux leads to significantly lower solar-wind speeds modeled by EUHFORIA. This effect is very strongly pronounced in 2012 (Figure 6a). We also note for 2012 the existence of a large number of low-latitude CHs surrounded by active regions, which possibly also influences the model performance by causing the magnetic topology to deviate strongly from being potential.

3.2. Identified Limitations of the Basic Setup of EUHFORIA

During testing of the modeled background solar wind, we identified some limitations of the present version of EUHFORIA that influence its performance. Herein we identify some of the limitations of the basic setup of the EUHFORIA 1.0.4, and a more detailed analysis will be presented in the follow-up article by Samara *et al.* (2020).

3.2.1. The Default Input Parameters of EUHFORIA

In order to set up benchmarks for solar-wind modeling with EUHFORIA we need to understand how different input parameters influence the modeled solar wind. Figure 9 shows the EUHFORIA model results for several days in March 2008 using different input parameters. We vary the resolution of the heliospheric model and the input density of the fast solar wind at the inner boundary compared to the default setting (Section 2.1 herein and Section 2.1.2. of Pomoell and Poedts, 2018). We find that a decrease of the solar-wind density by 50% (initial value is 300 cm^{-3} at 21.5 $R_{\odot}$) induces an increase of the modeled solar-wind speed from several percent up to 15% (absolute value depends on the part of the flow that is considered). Figure 9 also shows a comparison of the default, low-resolution runs (angular and radial resolution of 4° and 256 cells, respectively) and the high-resolution runs (2° and 512 cells, respectively). The higher-resolution runs result in an increased solar-wind speed (up

to about 20%) and in an earlier arrival time of the high-speed stream at 1 AU (up to several hours). If we compare the two extreme cases, the default EUHFORIA runs *i.e.* low resolution and high density, and the high-resolution and low-density runs, we find a shift of the arrival time of the fast flow of about -12 hours, and a significant increase of the solar-wind speed (from about 6% to more than 40%, depending on which part of the fast flow is considered). The results obtained indicate that the quality of the modeled fast solar wind varies a lot depending on the input parameters to the model. We note that when more than one parameter is modified the solar-wind speed changes in a non-linear manner and that the changes strongly depend on the flow considered. This brings forward the need for a detailed ensemble-parameter study that will provide a well-defined benchmark for solar-wind modeling with EUHFORIA (Samara *et al.*, 2020).

3.2.2. Open Flux and the Source-Surface Heights

Comparing CH sizes extracted from EUV observations, and modeled open-flux areas (*i.e.* CH areas) by PFSS using GONG synoptic magnetograms shows that on average CHs are underestimated in the model. It is found that the amount of modeled open flux is lower than actually observed, and open-flux areas show up smaller in angular width (Asvestari *et al.*, 2019). Failure in reliably modeling open magnetic flux has consequences for proper solar-wind modeling, in particular for the fast solar-wind flow originating from CH areas. This will not only result in an underestimation of the solar-wind speed but also might cause the fast flow to be too narrow, and hence, the flow may completely miss the Earth (Section 3.2.3). In a systematic test it was shown that changing the source-surface height (one of the default input parameters to EUHFORIA) significantly influences the modeled open flux and can even result in a shift of the position of the CH considered (Asvestari *et al.*, 2019).

3.2.3. Dependence on Shape and Location of CHs

While manually associating the observed and modeled solar-wind flows (Section 3.1.2), we recognized that the EUHFORIA performance is closely related also to the size, shape, and location of the CHs. The qualitative study of the CH characteristics and the quality of the modeled fast solar wind (Section 2.1) shows that for circular and equatorial CHs occurring during the low level of solar activity, EUHFORIA models well the associated fast flows. However, fast flows associated with narrow CHs elongated in longitude are rarely reproduced well by EUHFORIA. In the case of the narrow CHs elongated in latitude, the modeled solar wind is mostly underestimated, hence leading to a late arrival at the Earth. And when the solar wind is originating from low/high-latitude CHs (greater than $\pm 30°$) and/or the extensions of polar CHs, it will rarely be reproduced correctly by EUHFORIA. We also noticed that fast flows associated with patchy CHs, irrespective of their latitudes and longitudes, are poorly reproduced or not reproduced at all by EUHFORIA.

Furthermore, the fast flows originating from low-latitude CHs might pass South or North of the Earth (when the associated CHs are situated at the southern or northern solar hemisphere, respectively) and they will not be observed in the EUHFORIA time-series output at the Earth (see also Hofmeister *et al.*, 2018). In order to check this hypothesis, we have implemented virtual spacecraft around the Earth (separated by 4° ranging from $-12°$ to $+12°$ in latitude where 0° indicates Earth's position) and compared the modeled time series for all of these spacecraft. To amplify the effect, the values of time series at $+4°$, $+8°$, $+12°$ North of the Earth and $-4°$, $-8°$, $-12°$ South of the Earth were averaged and compared to *in-situ* data (see Figure 10). We note that the fast flow, starting on 9 March 2008 seems

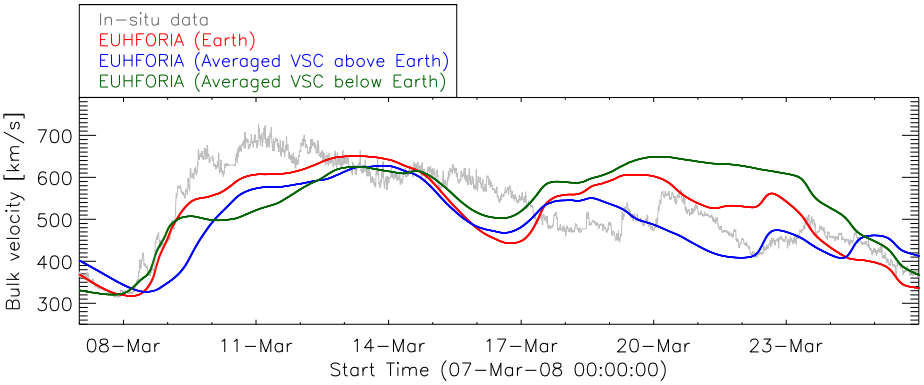

Figure 10 Combined EUHFORIA results in comparison to *in-situ* data (*gray*) for the same interval as in Figure 9. Earth (*red curve*) represents the EUHFORIA output for the Earth location. The *blue curve* is an average of combined EUHFORIA results for virtual spacecraft ($+4°$, $+8°$, $+12°$) North of the Earth and the *green curve* shows the averaged results for virtual spacecraft ($-4°$, $-8°$, $-12°$) South of the Earth.

to be reproduced well by EUHFORIA, by all three time series, *i.e.* North of the Earth, at the Earth and South of the Earth. This gives indications on the 3D extent of the fast flow that directly impacted the Earth, which is also visible in Figure 1 top-right panel. The solar wind observed starting from 19 March 2008 (Figure 10) originates from rather large low-latitude extensions of the southern polar CH. EUHFORIA models at the Earth a somewhat faster solar wind than observed by ACE (red curve), and significantly faster solar wind passing south of the Earth (green curve). In this case the fast flow only glanced the Earth while the main part of the fast solar wind passed South of the Earth. Studies of the 3D extent of the fast flows, using the virtual spacecraft, is among the main ongoing efforts for improving our knowledge on the solar wind and solar-wind modeling with EUHFORIA (Samara *et al.*, 2020).

4. Summary and Conclusions

In this article we present the first results of solar-wind modeling with the new EUHFORIA model. For the statistical study we employed the so-called basic setup of EUHFORIA 1.0.4 using default input parameters (Section 2.1). EUHFORIA currently provides daily modeled results using synoptic GONG magnetograms. In order to obtain a continuous time series of the background solar-wind parameters, the model outputs from consecutive days have to be combined. We developed a method to derive such a continuous profile from individual runs taking only the central part of the individual curves and combining them using a Gaussian weighting (Section 2.2).

We test the quality of the performance of EUHFORIA in solar-wind modeling by selecting two years of different solar-activity levels, *i.e.* 2008 and 2012. The analysis was focused on the comparison of the modeled solar wind for the two most important solar-wind plasma parameters, *i.e.* bulk speed and proton density, and ACE observations (Figures 5 and 6). As a general trend we notice an underestimation of the modeled solar-wind speed and an overestimation of the modeled density, in comparison with *in-situ* observations by ACE. The solar wind modeled by EUHFORIA matches better for the interval of the minimum solar activity in 2008 than for the year 2012 when the level of solar activity was high. We

conclude that this result is mostly originating from the better performance of the PFSS model (the main part of the EUHFORIA's coronal model) during low levels of solar activity.

To define the association between modeled and observed fast flows we applied an automatic peak-finding algorithm (Section 3.1.1). Using this algorithm we obtain 18 hits, 21 false alarms, and 25 misses for 2008 and 14 hits, 7 false alarms, and 24 misses for 2012. Uncertainty in the modeled arrival time of fast streams arises as a consequence of the frequently underestimated solar-wind speed modeled by EUHFORIA. Moreover, depending on the CH shape and location on the Sun, fast single flows may show multiple wind-speed maxima, which restricts the automatic peak-finding algorithm in finding the correctly matching pairs. By visual inspection (Section 3.1.2) we took into account all of these characteristics and assign more reliably the modeled and measured solar-wind flow pairs, and we obtained better statistics of 7 hits, 6 false alarms, and 12 misses for 2008 and 13 hits, no false alarms, and 18 misses for 2012.

Our statistics show that the quality of the modeled fast solar wind, obtained using the basic setup of EUHFORIA and the default input parameters, can be very variable. In the current study we identified some of the limitations of this setup. *E.g.* increasing the angular resolution from 4° to 2° can result in an increase of the solar-wind speed by up to 20% and that causes an earlier arrival of the fast solar-wind by up to several hours. Additionally, as expected, high-resolution runs show significantly more structures in the solar wind in comparison to the low-resolution ones. We also tested how the decrease of the fast solar-wind density from 300 cm^{-3} to 150 cm^{-3} influences the modeled solar wind and found that in the case of the lower input density EUHFORIA will model earlier arrival and larger amplitudes of the fast solar wind (Section 3.2.1). When combined, even only these two factors can lead to substantial errors in predictions. Detailed analysis on such limiting factors are presented in follow-up studies by Asvestari *et al.* (2019) and Samara *et al.* (2020).

The visual inspection of the CHs associated to the fast flows indicates that the shape and the location of the CHs play an essential role in the model performance (Section 3.2.3). We found that patchy, elongated, and narrow CHs are not well simulated by EUHFORIA's coronal model (*i.e.* PFSS misses open flux), which results in a poor model performance. We also found that the high-latitude ($> 30°$) CHs, often extensions of polar CHs, may be responsible for EUHFORIA modeling the fast flow passing North or South of the Earth (in a case of CHs on the northern and southern solar hemisphere, respectively). Therefore, it is very important to have EUHFORIA set up with included virtual spacecraft for all future studies of the solar-wind modeling by EUHFORIA. This will allow us to estimate the 3D extent of the fast flows and to understand if the fast flow just missed the Earth, passing South or North of it (Section 3.2.3).

In the study presented here we identified some of the limitations of the present version of EUHFORIA 1.0.4 that influences its performance, in particular during high levels of solar activity. We found that the dynamic behavior of the CHs, together with the complex coronal magnetic field, has a major role in the generation and propagation of the fast solar wind. Due to the complexity of the solar atmosphere, modeling of the fast solar wind is a very demanding task. We present first attempts to model the background solar wind with EUHFORIA, identified some of the limitations of the current setup of the model, and provide first examples of the parameter studies. The results presented bring forward the need for a detailed ensemble-parameter study that will provide a clear benchmark for the solar-wind modeling with EUHFORIA, but which goes beyond the scope of this article. The parameter studies, which are presently ongoing in the framework of the CCSOM project (www.sidc.be/ccsom/), will help us not only to improve modeling of the solar wind with EUHFORIA but also to improve EUHFORIA itself.

Acknowledgments Open access funding provided by Austrian Science Fund (FWF). J. Hinterreiter acknowledges the support by the Austrian Science Fund (FWF): P 31265-N27 (PI: T. Amerstorfer). M. Temmer acknowledges the support by the FFG/ASAP Program under grant No. 859729 (SWAMI). C. Verbeke is funded by the Research Foundation-Flanders, FWO SB PhD fellowship 11ZZ216N. E. Asvestari would like to acknowledge the financial support by the Finnish Academy of Science and Letters via the Postdoc Pool funding. C. Scolini was funded by the Research Foundation – Flanders (FWO) SB PhD fellowship no. 1S42817N. The work of E. Kilpua, E. Asvestari, and J. Pomoell has been achieved under the framework of the Finnish Centre of Excellence in Research of Sustainable Space (Academy of Finland grant number 312390). The validation of solar wind and CME modeling with EUHFORIA is being performed within the BRAIN-be project CCSOM (Constraining CMEs and Shocks by Observations and Modelling throughout the inner heliosphere; www.sidc.be/ccsom/). We acknowledge the ACE/SWEPAM instrument team and the ACE Science Center for providing the data.

Disclosure of Potential Conflicts of Interest The authors declare that they have no conflicts of interest.

References

Altschuler, M.D., Newkirk, G.: 1969, Magnetic fields and the structure of the solar corona. I: methods of calculating coronal fields. *Solar Phys.* **9**, 131. DOI. ADS.

Arge, C.N., Pizzo, V.J.: 2000, Improvement in the prediction of solar wind conditions using near-real time solar magnetic field updates. *J. Geophys. Res.* **105**(A5), 10465. DOI. ADS.

Arge, C.N., Odstrcil, D., Pizzo, V.J., Mayer, L.R.: 2003, Improved method for specifying solar wind speed near the Sun. In: Velli, M., Bruno, R., Malara, F., Bucci, B. (eds.) *Solar Wind Ten*, Am. Inst. Phys. **CS-679**, 190. DOI. ADS.

Asvestari, E., Heinemann, S.G., Temmer, M., Pomoell, J., Kilpua, E., Magdalenic, J., Poedts, S.: 2019, Reconstructing coronal hole areas with EUHFORIA and adapted WSA model: optimising the model parameters. arXiv. ADS.

Bougeret, J.-L., King, J.H., Schwenn, R.: 1984, Solar radio burst and *in situ* determination of interplanetary electron density. *Solar Phys.* **90**(2), 401. DOI. ADS.

Bussy-Virat, C.D., Ridley, A.J.: 2014, Predictions of the solar wind speed by the probability distribution function model. *Space Weather* **12**(6), 337. DOI. ADS.

Cranmer, S.R., Gibson, S.E., Riley, P.: 2017, Origins of the ambient solar wind: implications for space weather. *Space Sci. Rev.* **212**, 1345. DOI. ADS.

Den, M., Tanaka, T., Kubo, Y., Watari, S.: 2015, Three-dimensional MHD simulation of the solar wind from the solar surface to 400 solar radius using REPPU (REProduce Plasma Universe) code. In: *34th International Cosmic Ray Conference (ICRC2015)*, *International Cosmic Ray Conference* **34**, 184. ADS.

Feng, X., Yang, L., Xiang, C., Jiang, C., Ma, X., Wu, S.T., Zhong, D., Zhou, Y.: 2012, Validation of the 3D AMR SIP-CESE solar wind model for four Carrington rotations. *Solar Phys.* **279**(1), 207. DOI. ADS.

Garton, T.M., Gallagher, P.T., Murray, S.A.: 2018, Automated coronal hole identification via multi-thermal intensity segmentation. *J. Space Weather Space Clim.* **8**(27), A02. DOI. ADS.

Garton, T.M., Murray, S.A., Gallagher, P.T.: 2018, Expansion of high-speed solar wind streams from coronal holes through the inner heliosphere. *Astrophys. J. Lett.* **869**, L12. DOI. ADS.

Gressl, C., Veronig, A.M., Temmer, M., Odstrčil, D., Linker, J.A., Mikić, Z., Riley, P.: 2014, Comparative study of MHD modeling of the background solar wind. *Solar Phys.* **289**, 1783. DOI. ADS.

Heinemann, S.G., Temmer, M., Hofmeister, S.J., Veronig, A.M., Vennerstrøm, S.: 2018, Three-phase evolution of a coronal hole. I. 360° Remote sensing and *in situ* observations. *Astrophys. J.* **861**, 151. DOI. ADS.

Hofmeister, S.J., Veronig, A., Temmer, M., Vennerstrom, S., Heber, B., Vršnak, B.: 2018, The dependence of the peak velocity of high-speed solar wind streams as measured in the ecliptic by ACE and the STEREO satellites on the area and co-latitude of their solar source coronal holes. *J. Geophys. Res.* **123**, 1738. DOI. ADS.

Jaynes, A.N., Baker, D.N., Singer, H.J., Rodriguez, J.V., Loto'aniu, T.M., Ali, A.F., Elkington, S.R., Li, X., Kanekal, S.G., Fennell, J.F., Li, W., Thorne, R.M., Kletzing, C.A., Spence, H.E., Reeves, G.D.: 2015, Source and seed populations for relativistic electrons: their roles in radiation belt changes. *J. Geophys. Res.* **120**, 7240. DOI. ADS.

Jian, L.K., MacNeice, P.J., Taktakishvili, A., Odstrcil, D., Jackson, B., Yu, H.-S., Riley, P., Sokolov, I.V., Evans, R.M.: 2015, Validation for solar wind prediction at Earth: comparison of coronal and heliospheric models installed at the CCMC. *Space Weather* **13**, 316. DOI. ADS.

Karachik, N.V., Pevtsov, A.A.: 2011, Solar wind and coronal bright points inside coronal holes. *Astrophys. J.* **735**, 47. DOI. ADS.

Kilpua, E.K.J., Hietala, H., Turner, D.L., Koskinen, H.E.J., Pulkkinen, T.I., Rodriguez, J.V., Reeves, G.D., Claudepierre, S.G., Spence, H.E.: 2015, Unraveling the drivers of the storm time radiation belt response. *Geophys. Res. Lett.* **42**, 3076. DOI. ADS.

Kilpua, E.K.J., Balogh, A., von Steiger, R., Liu, Y.D.: 2017, Geoeffective properties of solar transients and stream interaction regions. *Space Sci. Rev.* **212**, 1271. DOI. ADS.

Linker, J.A., Mikić, Z., Biesecker, D.A., Forsyth, R.J., Gibson, S.E., Lazarus, A.J., Lecinski, A., Riley, P., Szabo, A., Thompson, B.J.: 1999, Magnetohydrodynamic modeling of the solar corona during whole Sun month. *J. Geophys. Res.* **104**, 9809. DOI. ADS.

MacNeice, P.: 2009, Validation of community models: identifying events in space weather model timelines. *Space Weather* **7**, S06004. DOI. ADS.

MacNeice, P., Elliott, B., Acebal, A.: 2011, Validation of community models: 3. Tracing field lines in heliospheric models. *Space Weather* **9**, S10003. DOI. ADS.

MacNeice, P., Jian, L.K., Antiochos, S.K., Arge, C.N., Bussy-Virat, C.D., DeRosa, M.L., Jackson, B.V., Linker, J.A., Mikic, Z., Owens, M.J., Ridley, A.J., Riley, P., Savani, N., Sokolov, I.: 2018, Assessing the quality of models of the ambient solar wind. *Space Weather* **16**(11), 1644. DOI. ADS.

McComas, D.J., Bame, S.J., Barker, P., Feldman, W.C., Phillips, J.L., Riley, P., Griffee, J.W.: 1998, Solar wind electron proton alpha monitor (SWEPAM) for the advanced composition explorer. *Space Sci. Rev.* **86**, 563. DOI. ADS.

McGregor, S.L., Hughes, W.J., Arge, C.N., Owens, M.J.: 2008, Analysis of the magnetic field discontinuity at the potential field source surface and Schatten current sheet interface in the Wang-Sheeley-Arge model. *J. Geophys. Res.* **113**, A08112. DOI. ADS.

McGregor, S.L., Hughes, W.J., Arge, C.N., Owens, M.J., Odstrcil, D.: 2011, The distribution of solar wind speeds during solar minimum: calibration for numerical solar wind modeling constraints on the source of the slow solar wind. *J. Geophys. Res.* **116**, A03101. DOI. ADS.

Merkin, V.G., Lyon, J.G., Lario, D., Arge, C.N., Henney, C.J.: 2016, Time-dependent magnetohydrodynamic simulations of the inner heliosphere. *J. Geophys. Res.* **121**(4), 2866. DOI. ADS.

Nakagawa, Y., Nozawa, S., Shinbori, A.: 2019, Relationship between the low-latitude coronal hole area, solar wind velocity, and geomagnetic activity during solar cycles 23 and 24. *Earth Planets Space* **71**, 24. DOI. ADS.

Odstrčil, D., Pizzo, V.J.: 1999, Three-dimensional propagation of CMEs in a structured solar wind flow: 1. CME launched within the streamer belt. *J. Geophys. Res.* **104**, 483. DOI. ADS.

Odstrcil, D., Riley, P., Zhao, X.P.: 2004, Numerical simulation of the 12 May 1997 interplanetary CME event. *J. Geophys. Res.* **109**, A02116. DOI. ADS.

Opitz, A., Karrer, R., Wurz, P., Galvin, A.B., Bochsler, P., Blush, L.M., Daoudi, H., Ellis, L., Farrugia, C.J., Giammanco, C., Kistler, L.M., Klecker, B., Kucharek, H., Lee, M.A., Möbius, E., Popecki, M., Sigrist, M., Simunac, K., Singer, K., Thompson, B., Wimmer-Schweingruber, R.F.: 2009, Temporal evolution of the solar wind bulk velocity at solar minimum by correlating the stereo a and b plastic measurements. *Solar Phys.* **256**(1), 365. DOI. ADS.

Owens, M.J., Riley, P., Horbury, T.S.: 2017, Probabilistic solar wind and geomagnetic forecasting using an analogue ensemble or "similar day" approach. *Solar Phys.* **292**(5), 69. DOI. ADS.

Owens, M.J., Spence, H.E., McGregor, S., Hughes, W.J., Quinn, J.M., Arge, C.N., Riley, P., Linker, J., Odstrcil, D.: 2008, Metrics for solar wind prediction models: comparison of empirical, hybrid, and physics-based schemes with 8 years of L1 observations. *Space Weather* **6**, S08001. DOI. ADS.

Owens, M.J., Challen, R., Methven, J., Henley, E., Jackson, D.R.: 2013, A 27 day persistence model of near-Earth solar wind conditions: a long lead-time forecast and a benchmark for dynamical models. *Space Weather* **11**, 225. DOI. ADS.

Paulikas, G.A., Blake, J.B.: 1979, Effects of the solar wind on magnetospheric dynamics: energetic electrons at the synchronous orbit. *Am. Geophys. Union Geophys. Monogr* **21**, 180. DOI. ADS.

Pomoell, J., Poedts, S.: 2018, EUHFORIA: European heliospheric forecasting information asset. *J. Space Weather Space Clim.* **8**(27), A35. DOI. ADS.

Reiss, M.A., Temmer, M., Veronig, A.M., Nikolic, L., Vennerstrom, S., Schöngassner, F., Hofmeister, S.J.: 2016, Verification of high-speed solar wind stream forecasts using operational solar wind models. *Space Weather* **14**, 495. DOI. ADS.

Richardson, I.G., Cane, H.V.: 2010, Near-Earth interplanetary coronal mass ejections during solar cycle 23 (1996 – 2009): catalog and summary of properties. *Solar Phys.* **264**, 189. DOI. ADS.

Richardson, I.G., Cane, H.V.: 2012, Near-Earth solar wind flows and related geomagnetic activity during more than four solar cycles (1963 – 2011). *J. Space Weather Space Clim.* **2**(27), A02. DOI. ADS.

Riley, P., Ben-Nun, M., Linker, J.A., Owens, M.J., Horbury, T.S.: 2017, Forecasting the properties of the solar wind using simple pattern recognition. *Space Weather* **15**(3), 526. DOI. ADS.

Rotter, T., Veronig, A.M., Temmer, M., Vršnak, B.: 2012, Relation between coronal hole areas on the Sun and the solar wind parameters at 1 AU. *Solar Phys.* **281**, 793. DOI. ADS.

Samara, E., Magdalenic, J., Rodriguez, L., Heinemann, S.G., Hinterreiter, J., Pomoell, J., Poedts, S.: 2020, *Astron. Astrophys.*, in preparation for submission to Astron. Astrophys.

Schatten, K.H., Wilcox, J.M., Ness, N.F.: 1969, A model of interplanetary and coronal magnetic fields. *Solar Phys.* **6**, 442. DOI. ADS.

Schwenn, R.: 2006, Space weather: the solar perspective. *Liv. Rev. Solar Phys.* **3**, 2. DOI. ADS.

Scolini, C., Verbeke, C., Poedts, S., Chané, E., Pomoell, J., Zuccarello, F.P.: 2018, Effect of the initial shape of coronal mass ejections on 3-D MHD simulations and geoeffectiveness predictions. *Space Weather* **16**, 754. DOI. ADS.

Scolini, C., Rodriguez, L., Mierla, M., Pomoell, J., Poedts, S.: 2019, Observation-based modelling of magnetised coronal mass ejections with EUHFORIA. *Astron. Astrophys.* **626**, A122. DOI.

Shiota, D., Kataoka, R., Miyoshi, Y., Hara, T., Tao, C., Masunaga, K., Futaana, Y., Terada, N.: 2014, Inner heliosphere MHD modeling system applicable to space weather forecasting for the other planets. *Space Weather* **12**(4), 187. DOI. ADS.

Temmer, M., Hinterreiter, J., Reiss, M.A.: 2018, Coronal hole evolution from multi-viewpoint data as input for a STEREO solar wind speed persistence model. *J. Space Weather Space Clim.* **8**(27), A18. DOI. ADS.

Temmer, M., Reiss, M.A., Nikolic, L., Hofmeister, S.J., Veronig, A.M.: 2017, Preconditioning of interplanetary space due to transient CME disturbances. *Astrophys. J.* **835**(2), 141. DOI. ADS.

Tsurutani, B.T., Gonzalez, W.D.: 1987, The cause of high-intensity long-duration continuous AE activity (HILDCAAs): interplanetary Alfvén wave trains. *Planet. Space Sci.* **35**, 405. DOI.

Tsurutani, B.T., Gonzalez, W.D., Gonzalez, A.L.C., Guarnieri, F.L., Gopalswamy, N., Grande, M., Kamide, Y., Kasahara, Y., Lu, G., Mann, I., McPherron, R., Soraas, F., Vasyliunas, V.: 2006, Corotating solar wind streams and recurrent geomagnetic activity: a review. *J. Geophys. Res.* **111**, A07S01. DOI. ADS.

van der Holst, B., Sokolov, I.V., Meng, X., Jin, M., Manchester, W.B. IV, Tóth, G., Gombosi, T.I.: 2014, Alfvén wave solar model (AWSoM): coronal heating. *Astrophys. J.* **782**(2), 81. DOI. ADS.

Venzmer, M.S., Bothmer, V.: 2018, Solar-wind predictions for the Parker Solar Probe orbit. Near-Sun extrapolations derived from an empirical solar-wind model based on helios and OMNI observations. *Astron. Astrophys.* **611**, A36. DOI. ADS.

Vršnak, B., Temmer, M., Veronig, A.M.: 2007, Coronal holes and solar wind high-speed streams: I. forecasting the solar wind parameters. *Solar Phys.* **240**, 315. DOI. ADS.

Webb, D.F., Howard, T.A.: 2012, Coronal mass ejections: observations. *Liv. Rev. Solar Phys.* **9**, 3. DOI. ADS.

Wiengarten, T., Kleimann, J., Fichtner, H., Cameron, R., Jiang, J., Kissmann, R., Scherer, K.: 2013, MHD simulation of the inner-heliospheric magnetic field. *J. Geophys. Res.* **118**(1), 29. DOI. ADS.